Aeroelastic Calculation of Innovative Non-conventional Aircraft with Swinging Canard Surface

Wojciech C. Chajec[1]

(Received: Nov. 25, 2013. Revised: Jan. 9, 2014. Accepted: June 25, 2014)

Abstract
A flutter computational analysis of experimental (concept demonstrator) semi-canard aircraft named EM-12 Magosia II is presented. Differently from other canards, the aircraft designed by Edward Margaski is equipped with a forward surface that can swing freely on transverse axis. This surface is controlled only by tabs located behind its trailing edge. The tabs are mechanically connected with sticks and spring trim in the cockpit. This solution - according to designer's idea - should have advantages of canard system and should not have canard's defects. The swept wing of the Magosia II is equipped with ailerons and split flaps. The fin with split rudder is located at each wing tip. The aeroplane is powered by piston engine with pushing propeller. The design dive speed of this aircraft is V_D= 290 km/h.

The flutter analysis has been performed with the MSC/Nastran system using beam-like FEM model of structure and DLM aerodynamic model. The FEM model of the structure contains the control systems' model and it was verified by comparison with results of both static tests and GVT. Among static properties verification, the test of wing torsional rigidity has been made as in [1]. All ground tests were provided by Silesian Science and Technology Center of Aerospace Ltd. in Czechowice-Dziedzice. As a result of flutter computation the wing torsional-bending flutter modes were determined which are typical for a swept wing aircraft. Three tabs configuration were examined. In both cases of heave tabs the anti-symmetric flutter mode with canard rolling and torsion appears below maximal dive speed of the aircraft.

1 Introduction

The EM-12 Magosia II (Fig. 1c) is an experimental, semi-canard, low-cost aircraft designed and built by Edward Margaski. Differently from ordinary canards, the EM-12 forward surface (canard) can swing freely on transverse axis. This surface is fully mass balanced and controlled only by tabs located approximately 200 mm behind trailing edge. The tabs are mechanically connected with control sticks and spring trim in a cockpit.

The main part of the wing (up to aileron mid station) and some other elements of the Mangosia II were adopted from the Mangosia (Fig. 1b) that was a powered version of the MDM-1 Fox (Fig. 1a) famous aerobatic sailplane. The wing is equipped with Friese-ailerons, balanced as in the Fox sailplane. The wing of the Magosia II is swept and contains split flaps. The fin with split rudder is located at each wing tip. The aircraft is powered by piston Rotax engine with pushing propeller. The maximal take-off mass of this aircraft is 800 kg, wing span 9.09 m, design dive speed V_D = 290 km/h.

A 1:2.5 scale RC model was successfully tested in flight, including some aerobatic figures. Due to swept wing and freely swinging forward surface, this airplane is very interesting for analysts. The dynamic aeroelastic analysis was performed up to June 2013 with MSC/Nastran [4] system using beam-like FEM model of structure and DLM aerodynamic model. The flight tests were planned in summer 2013, but during the take-off, the pilot had a problem to stabilize the risen front landing gear, so the aircraft did not fly in 2013. The aircraft will be further developed by designer (tests with auxiliary classic tail, opimization of control efficiency and control forces on stick).

[1] Instytut Lotnictwa (Institute of Aviation) Al. Krakowska 110/114, 02-256 Warszawa, Poland

doi:10.3293/asdj.2013.24

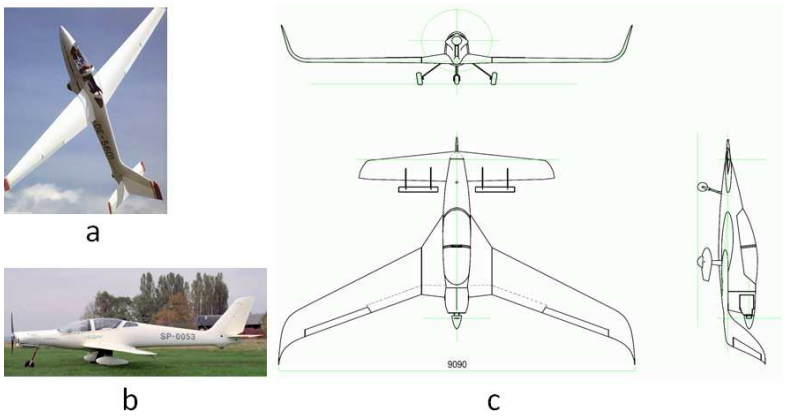

Figure 1: a) MDM-1 Fox aerobatic glider; b) Mangosia powered sailplane; c) EM-12 Mangosia II aircraft.

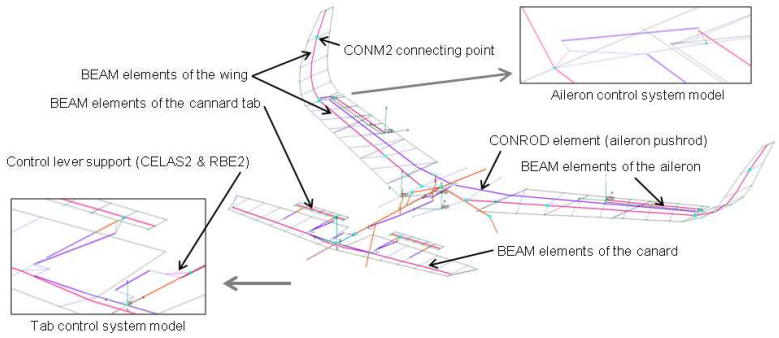

Figure 2: The beam-like FEM model of the EM-12 Mangosia II aircraft.

2 Analytical and Numerical Models

The MSC/Nastran FEM model of the structure is simple and beam-like. It contains the Nastran BEAM elements (lines in magenta on Fig. 2) for modelling of stiffness and mass of main aircraft surfaces like wing, ailerons, canard and canard tabs. The BAR elements (orange) create the simple model of fuselage, landing gear, tabs support and sticks. However the BEAM and BAR elements include the mass data, the FEM model of EM-12 a/c contains also some concentrated mass elements, CONM2 (cyan squares in the CONM2 connection nodes, offsets are not shown). The split flaps and split rudders are rigid and irreversibly controlled, so each one is simulated only by a CONM2 mass element that is rigidly connected to wing beam.

For better visualization the model contains also the slave nodes that are connected with other nodes by rigid elements (blue). These slave nodes are located on the leading and trailing edges and are connected by dummy PLOTEL elements (grey).

From author's experience (especially from flutter calculation of the SZD-56 Diana sailplane, [3], see also [4, 5, 7]) it is known that, in case of mechanically controlled light aircraft and sailplanes, the FEM model should contain also the masses of most important control system elements as control wheels, sticks, push-rods, bob-weights, mass balances, test equipment etc. This model can take into consideration the kinetic energy of the control system including couplings between movements of aircraft assembly (as a wing) and the control system's masses (as a pushrod). The pushrods are replaced by the CONROD elements (violet segments) with mass, rigid for tension and flexible for torsion. The control system levers are simulated by RBE2 (blue) rigid elements. Thanks to this approach to modeling, the normal modes, in which the control system is acting as a mechanism, can be obtained. Nevertheless, the normal modes, in which the control system is acting as a spring, are also very important in the flutter calculation. The control system flexibility is modeled by lever support flexibility (mainly, CELAS2 elements, pink) and by CONROD elements' longitudinal stiffness.

Flutter type	k_{max} [-]	$2b$ [m]	f_{max} [Hz]
Wing flutter (high aspect ratio wing)	0.8	1.015	20.2
Wing flutter (low aspect ratio wing)	1.1	1.015	27.8
Canard flutter (canard treated as a horizontal empennage)	0.55	0.715	19.7
Canard flutter (canard treated as a high aspect ratio wing)	0.8	0.649	31.6
Canard flutter (canard treated as a low aspect ratio wing)	1.1	0.649	43.5

Table 1: The highest flutter frequency of EM-12 according to [2] for V_D = 290 km/h = 80.6 m/s.

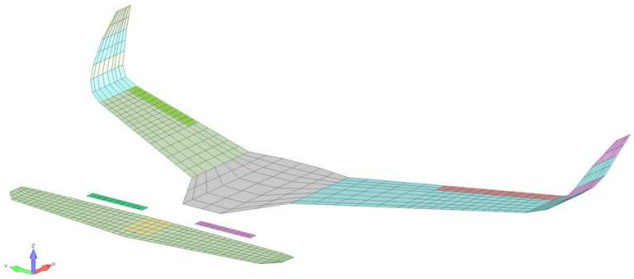

Figure 3: The aerodynamic model for basic tabs-variant of the EM-12 (particular interpolation area are colored).

The analytical FEM model was prepared using a spreadsheet in MS Excel with VB-macros, found to be an easily modifiable form. It is also possible to use the stiffness and mass properties along the BEAM elements formulated as a function of some linear argument, e.g. a spanwise station. The FEMAP post-processor was used only for FEM and aerodynamic model visualization as well as for the normal modes presentation. Apart from FEMAP some author's (and his coworkers' from PZL-Mielec) own programs [4, 7] were used for the presentation of the flutter computation results. For example the SOWY program makes the g(V) and f(V) flutter diagrams, TRANRYS and RYSH programs prepare and animate the normal and flutter modes, the AER2QUAD program converts aerodynamic boxes CAERO1 from NASTRAN *.f06-file (SOL 145 with PARAM OPPHIPA=1) to QUAD4-elements, nodes and their displacements.

The frequency limit for flutter computation was determined according to statistical classification of flutter incidents [2] (Fig. 4). These statistical data does not contain canard aircraft, but can be used for estimation, see Table 1. The maximal dive speed, V_D without safety margin was used for calculation, although the aircraft, with a status of concept demonstrator, most probably will be tested at limited speed. Finally, all normal modes with frequency up to 30 Hz were taken into account.

The FEM model was verified by ground tests made by *lskie Centrum Naukowo-Technologiczne Przemysu Lotniczego Sp.zo.o.* (Silesian Science and Technology Center of Aerospace, Ltd.) in Czechowice-Dziedzice. To simulate the aircraft support during tests the single point constraints (SPC) and springs (CELAS2) are used. The analytical model verification based on static and GVT results will be described in the sections 3 and 4.

The numerically determined normal vibration modes of free aircraft were coupled by the connecting SPLINE1 elements with typical DLM model of unsteady aerodynamics. It contains only the CAERO1 boxes and does not contain the fuselage body, see Fig. 3.

The flutter computation was provided using PK method for air density at sea level. The modal damping coefficients are not known and were omitted. The flutter computation results are presented as g(V) and f(V) diagrams, where the V is flight speed in km/h. The reduced frequency, k on the diagrams, is related to conventional chord value 2b=1m. The most important flutter curves are identified by colors, markers and labels. The diagrams g(V) contain a horizontal lines at g=0.02 and g = 0.03 for typical, predicted global structural damping.

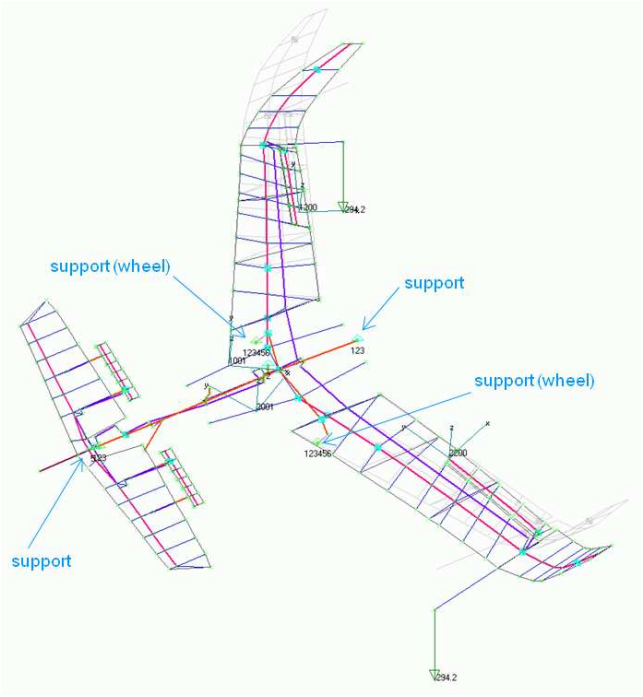

Figure 4: The numerical simulation of the static wing test with loads 30 kg (294 N; undeformed shape is grey)

Table 2: Results of static test and its numerical simulation (final wing stiffness model) loaded with 30 kg.

	y [mm]	x_1 [mm]	x_2 [mm]	D_x [mm]	$D_{z,1}$ [mm]	$D_{z,2}$ [mm]	a [mrad]	$D_{z,1}$ [mm]	$D_{z,2}$ [mm]	a [mrad]
4R	3862	4278.9	5161.6	882.7	-11.5	-22	**11.9**	-10.7	-22.2	**13.0**
3R	2870	3706.4	4753.6	1047.2	-5	-12	6.7	-3.6	-12.4	8.41
2R	1892	3141.9	4347.8	1205.9	0	-5.5	4.6	-0.5	-5.7	4.17
1R	920	2580.5	3947.9	1367.4	1	-2	2.2	0.4	-1.1	1.06
1L	-920	2580.5	3947.9	1367.4	-1	-0.5	-0.4	-0.4	0.2	-0.42
2L	-1892	3141.9	4347.8	1205.9	-4	-3	-0.8	-2.4	0.1	-2.02
3L	-2870	3706.4	4753.6	1047.2	-9	-6	-2.9	-6.6	-2.0	-4.45
4L	-3862	4278.9	5161.6	882.7	-16	-7	**-10.2**	-11.8	-4.4	**-8.33**

3 Verification of Wing Stiffness Using Static Test

The test of wing torsional rigidity was described in the NACA Report 45 [1]. During test the aircraft was standing on the wheels. The additional support points were at nose and rear part of fuselage, Fig. 4. The wings were loaded with 15 and 30 kg forces. The displacements were measured in the four section of each wing.

The Table 2 presents a comparison between measured and computed displacements. The results are not identical. One of the reasons of the discrepancy was the rigid body movement. The torsional stiffness of wing is confirmed, because the measured and computed torsional angles (right wing tip relative to left wing tip) are comparable: $11.9 + 10.2 = 22.1$ vs. $13.0 + 8.33 = 21.33$.

4 Validation of the FEM model Using GVT Results

The simplified ground vibration test of this aircraft was performed on November 2012 using the LMS measurement system, Fig. 5. During the test the aircraft did not have the mass balance on the tabs, but the whole canard assembly was balanced. It included rear pilot dummy mass and did not contain any fuel mass. The sticks and pedals were free.

The results of the EM-12 GVT were used to validate the theoretical computational FEM dynamic model by comparison of the measured and calculated normal vibration modes (Table 3). The analytical mass model was adequate

Figure 5: The EM-12 aircraft during simplified GVT.

for GVT configuration (no fuel, rear pilot dummy mass, no tabs mass balance), but the acceleration sensors' and cable masses were not taken into account. It was provided with elements (SPC, CELAS2) that simulate the aircraft's wheels contact with the ground.

5 Flutter computation for basic aircraft configuration

The main computational case labeled 62 is related to aircraft as during GVT, but in free-free condition (as during flight) and with maximal fuel mass.

In this computational case the frequencies of the normal modes 1-8 are equal to 0 (six rigid body modes of free aircraft, canard swinging and mechanism mode: sticks rolling + aileron deflection). As a result of spring trim application, the normal frequency of tab deflection, in which the control system is acting as a mechanism, is 6.1 Hz.

The Fig. 6 presents the 12^{th} normal mode, f = 9.015 Hz. To prove the connection between the structural and aerodynamic models, the displacements of the both models are shown.

From another computation it is known that the critical speed of flutter modes C and L depends on the wing's torsional stiffness. It was also computed the pilot's influence (by mass and support stiffness added to stick) and the trim spring alteration. These alterations of analytical model give a moderate influence to flutter computation results.

6 Tab variants

The alternate tabs design solutions shown in the Fig. 11 were introduced to optimize the aircraft longitudinal control. The effectiveness of the tabs variants a) and b) was too large, and the forces on control stick were too small, so the aircraft - according to preliminary tests - was difficult to control. The solution c) - large tabs equipped with anti-flettner was introduced to increase the forces on stick. The surface of tabs c) is bigger than in b), so -additionally - the localized in fuselage nose control system's lever was altered from 90/90 to 130/30 (black bar on Fig. 10). The tabs angles are in the solution c) over 4.3-time smaller than in b). After tests the canard longitudinal control will be further optimized by the designer.

6.1 Canard With Balanced Tabs

The computational case applying to aircraft with tabs fully static balanced by mass 0.6 kg each (Fig. 11b) was labeled 32. The flutter diagrams for this case are shown on Fig. 12. In this case appeared additionally the flutter mode M described below in Figure 13. It is a result of the mass added behind the canard elastic axis. The critical speeds of flutter modes B, C and L are a bit higher than before tab balancing (case 62).

Table 3: Comparison of calculated and measured normal modes. The modes critical for flutter are highlighted.

No.	f, [Hz]	m, [kgm^2]	Description of mode shapes (computational case **52**)	Meas. [Hz]
1	0	11.59	Canard pitch deflection (a mechanism)	0
2	0	0.44	Aileron deflection with sticks rolling (the control system is acting as a mechanism)	0
3	0.92	69.62	Yawing of rigid aircraft on wheels	X
4	1.12	464	Longitudinal vibration of rigid aircraft on wheels	X
5	1.61	58.58	Rolling of rigid aircraft on wheels	X
6	2.44	59.75	Pitching of rigid aircraft on wheels	X
7	3.33	91.61	Vertical vibration and rolling (mixed)	X
8	4.27	37.6	Vertical vibration and pitching (mixed)	X
9	5.80	4.72	1^{st} symmetrical wing bending (2 nodes per wing span), tabs deflection with sticks	5.93
10	6.10	0.53	Tabs deflection with sticks (the control system is acting as a mechanism, but it exists a trim stiffness)	6.12
11	6.89	4.44	Fuselage torsion (with canard rolling)	6.88
12	10.30	12.35	1^{st} anti-symmetrical wing bending (3 nodes per wing span), - canard rolling	13.93
13	10.34	8.96	Symmetrical wing torsion + 1^{st} symmetrical wing bending in the chord plane	13.82
14	11.11	12.37	Anti-symmetrical wing torsion, canard yawing	10.91
15	12.97	3.33	Anti-symmetrical canard torsion	14
16	13.05	3.37	1^{st} symmetrical canard bending (2 nodes per wing span)	12.85
17	14.81	8.55	Canard yawing	13.97
18	17.83	10.84	2^{nd} sym. wing bending (4 nodes per wing span), 1^{st} symmetrical canard bending	15.91
19	18.35	4.82	2^{nd} symmetrical canard torsion, mass balance pitching, tabs torsion	18.5
20	18.64	6.48	1^{st} symmetrical wing bending in the chord plane - symmetrical wing torsion	
21	20.08	4.32	1^{st} symmetrical canard bending in the chord surface	20.8
22	20.97	5.34	1^{st} symmetrical canard bending in the chord plane + other	
23	22.60	12.62	Anti-symmetrical wing bending and torsion	
24	26.49	0.47	Tabs opposite to sticks, ailerons opposite to sticks (the control systems are acting as a springs)	
25	27.01	3.83	Stick pitching opposite to tabs deflection and torsion(the control system is acting as a spring), high wing bending and torsion	28.9
26	27.12	5.88	High wing bending and torsion	
27	28.66	0.61	Symetrical aileron deflection + torsion	27..29
28	29.06	1.36	High symmetrical canard torsion with tabs rolling	
29	29.31	0.67	Anti-symetrical aileron deflection + torsion, symetrical tabs bending	33

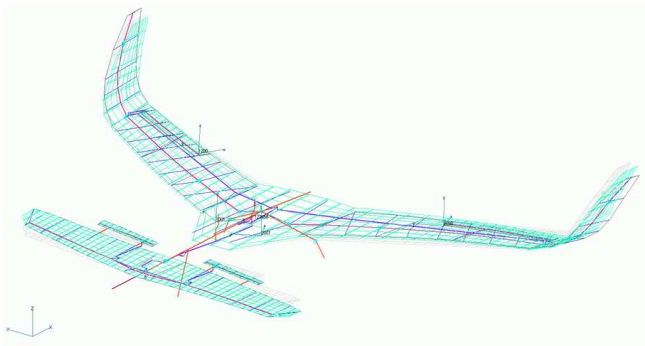

Figure 6: The structural and aerodynamic (cyan) models displacements in the 12^{th} normal mode, computational case 62 (grey - undeformed shape).

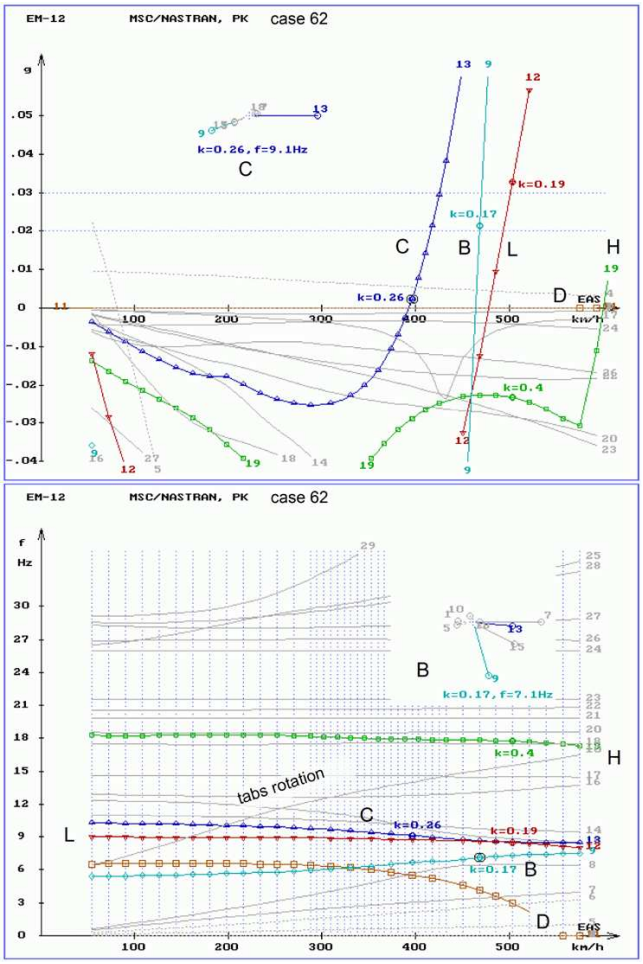

Figure 7: Flutter g(V) and f(V) diagrams for case 62 (basic tabs, sticks and pedals free).

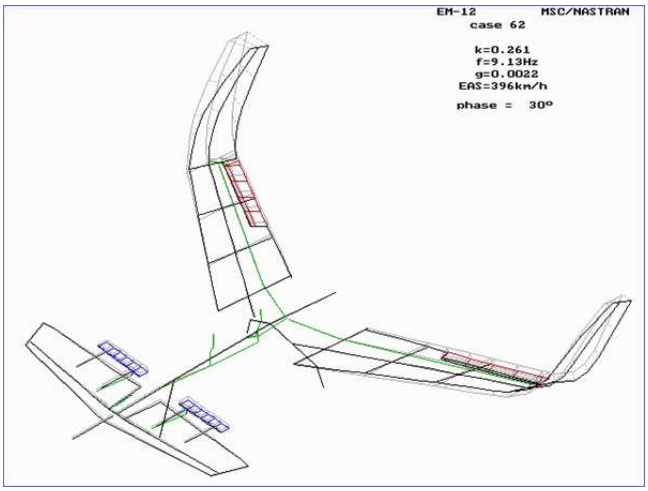

Figure 8: the critical flutter speed is higher than 390 km/h. The main flutter modes C, B and L are described in Figure 9-11.

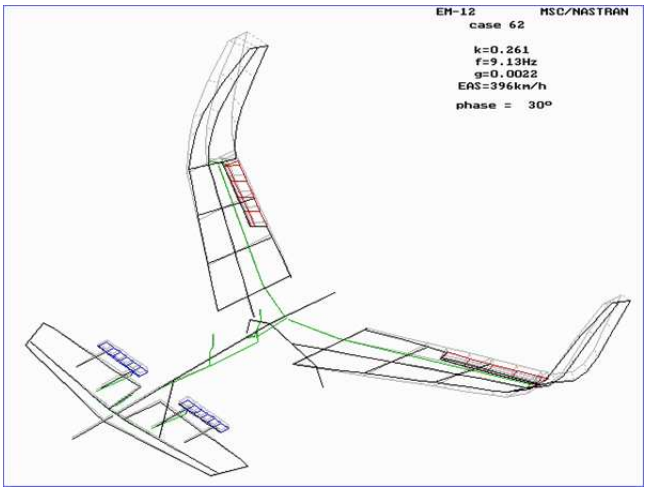

Figure 9: Case C: Symmetrical wing torsional-bending flutter, f=9.1 Hz, V_{cr}= 393 km/h (structural damping not taken into account), typical for swept wing. The flutter critical speed depends on wing torsional stiffness.

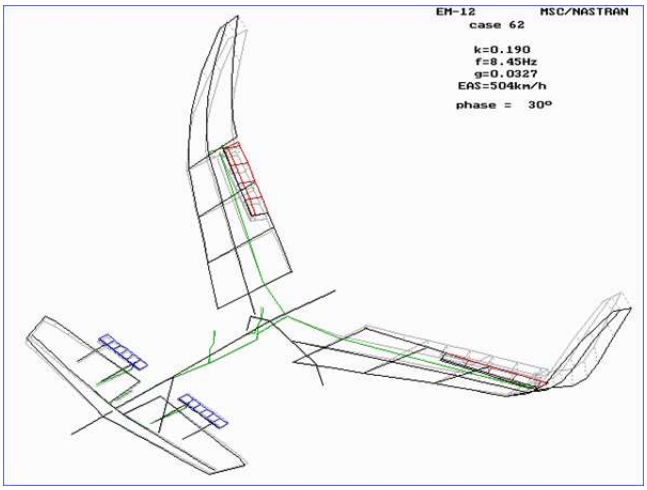

Figure 10: Case L: Anti-symmetrical wing torsional-bending flutter, f=8.6 Hz, V_{cr}= 478 km/h, typical for swept wing. The flutter critical speed depends on wing torsional stiffness.

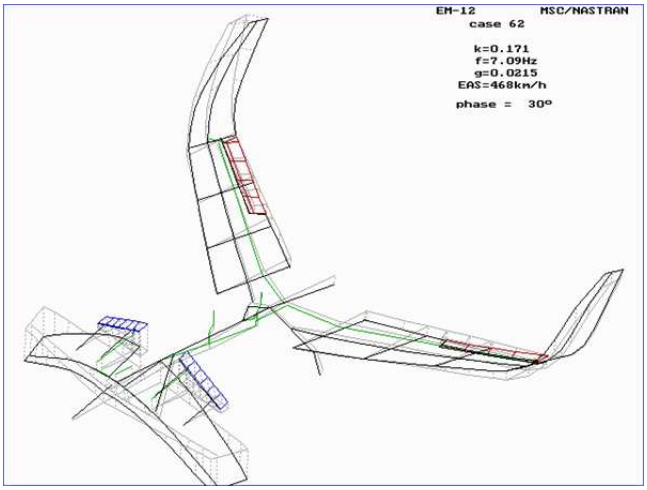

Figure 11: Case B: Symmetrical fuselage bending flutter with canard bending and deflection as well as wing torsion and bending, f=7.0 Hz, V_{cr}=464 km/h.

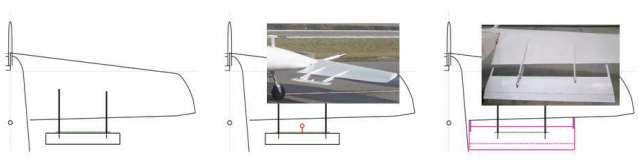

Figure 12: Tabs variants: a) basic (as during GVT), b) basic with mass balance, c) large tabs with anti-flettner.

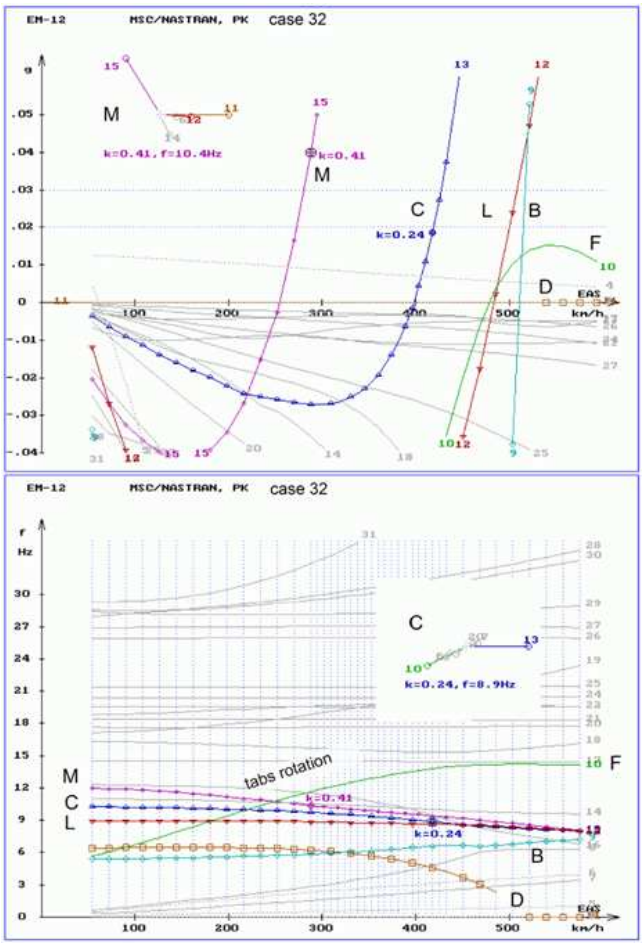

Figure 13: Flutter g(V) and f(V) diagrams for case 32 (balanced small tabs, sticks and pedals free).

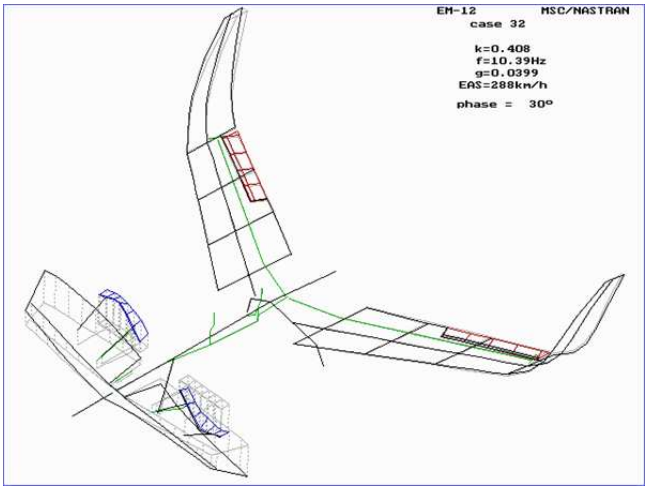

Figure 14: Case M: Anti-symmetrical torsion-bending-rolling canard flutter with bending of the tabs, f=10.4 Hz, V_{cr}=254 km/h (structural damping not taken into account). The flutter critical speed depends on canard torsional stiffness and on the mass behind canard torsional axis.

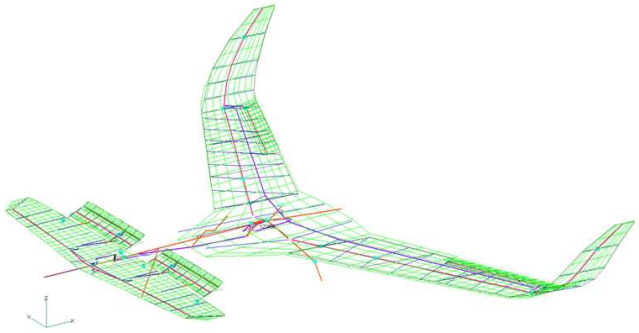

Figure 15: Structural and aerodynamic (green) models displacements in the 11^{th} normal mode, f =7.1 Hz (tabs rotation + stick pitching on trim spring). The modified control lever is marked in black.

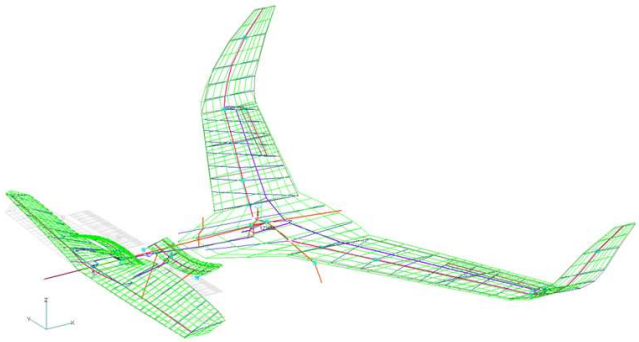

Figure 16: Structural and aerodynamic (green) models displacements in the 15th normal mode, f=11.5 Hz (canard anti-symmetrical torsion with tabs bending), computational case 45.

6.2 Canard With Large Tabs

The computational cases concerning aeroplane equipped with large tabs (Fig. 11c) were labeled 63 (preliminary analysis, control system as in case 62) and 45 (after control lever change). The Fig. 14. and 15. present the model and displacements of the selected normal modes for the 45 computational case. The rotation of tabs normal frequencies, f_{T1} (mechanism) and f_{T2} (control system is acting as a spring) are: case 63: 4.1 Hz and 20.7 Hz; case 45: 7.1 Hz and 17.6 Hz. The flutter computation results for cases 63 and 45 are shown on Fig. 16.

The hinge moments on the large tabs and the forces on control sticks for case 63 are greater than ones for small tabs variant, case 62, so the slope of a curve tabs rotation frequency vs. speed on the Fig. 16a is bigger than this one on Fig. 9. After control lever alteration, Fig. 16b, the slope is close to the slope on Fig. 12.

The important question before the first flight is the possibility of pilot induced oscillation. The PK flutter computation method is used and the rigid

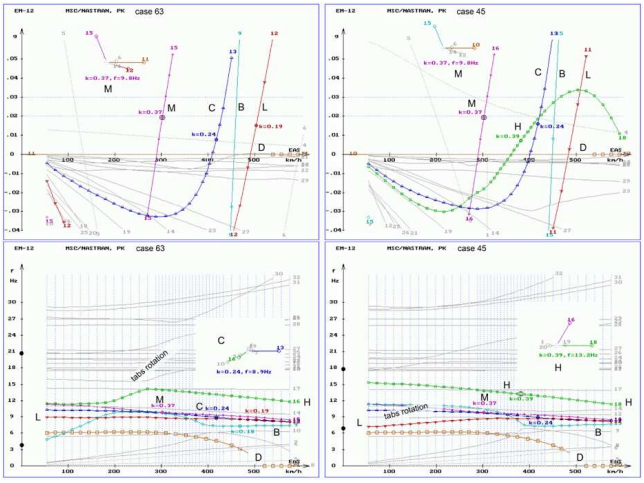

Figure 17: Flutter diagrams (large tabs with anti-flettner; sticks and pedals free): a) case 63 (control system as in case 62), b) case 45 (after control lever change).

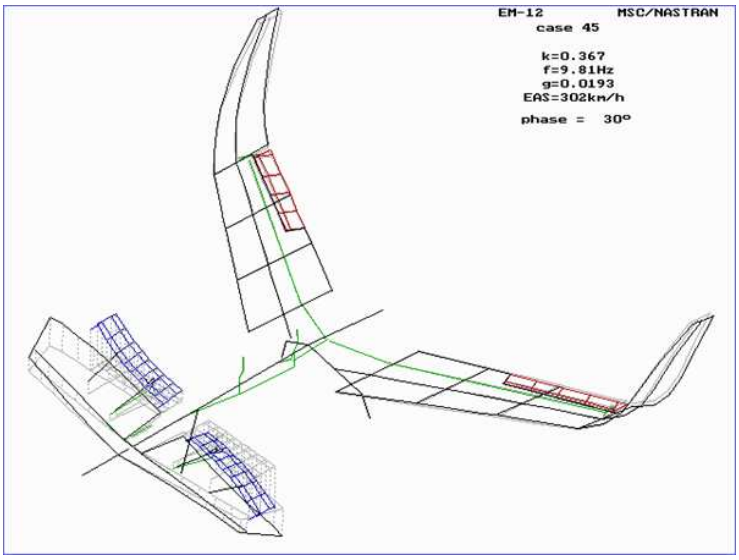

Figure 18: Case M: Anti-symmetrical torsion/bending/rolling canard flutter with bending of the tabs, f = 9.9 Hz , V_{cr}=290 km/h (structural damping was not taken into account). It is a side effect of large tab mass, but the V_{cr} is higher than this one in the Case 32.

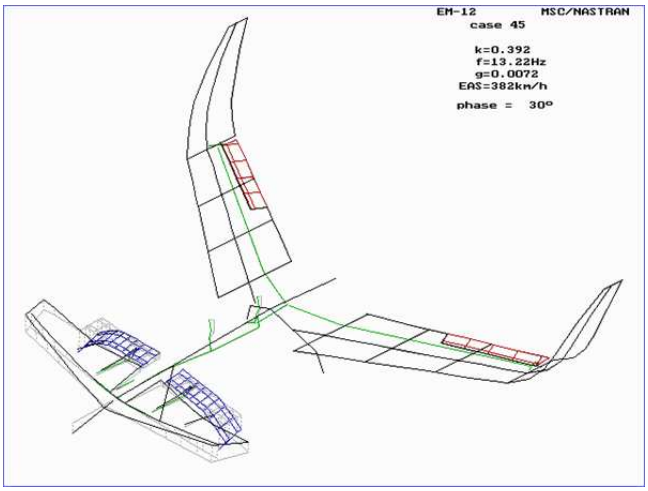

Figure 19: Case H: Symmetrical canard torsional-bending flutter with tabs bending, f=13.4 Hz, V_{cr}=360 km/h. The H flutter mode was not important in the previous computation case.

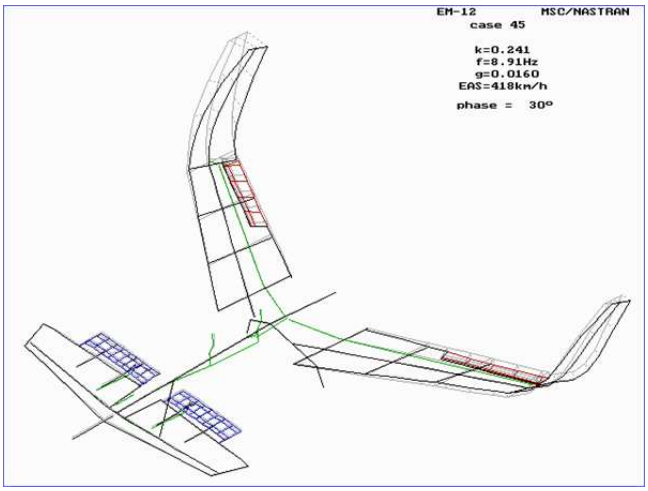

Figure 20: Case C: Symmetrical wing torsional-bending flutter, f =9.0 Hz, V_{cr}= 401 km/h, typical for swept wing. The critical flutter speed is by 8 km/h higher than this one for the basic tabs configuration, computational Case 62.

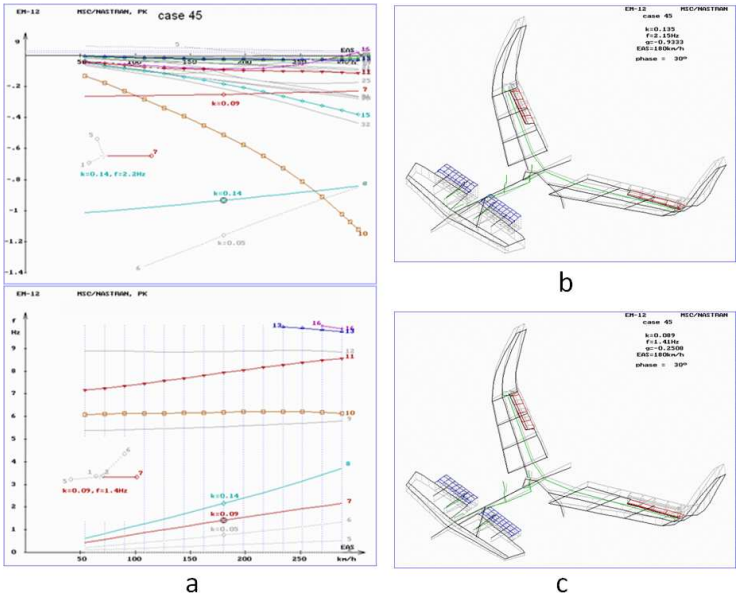

Figure 21: The low frequency part of the g-f-V diagram for computational case 45 and selected compound modes. A) The g-f-V diagram, b) Compound mode No. 8 at 180 km/h (k=0.14) and c) Compound mode No. 7 at 180 km/h (k=0.09).

body modes are taken into account, so it is possible to obtain a simplified (small disturbances theory) answer to the question. To this goal the compound modes with low frequency and control surfaces' movement are investigated. The flight speed, 180 km/h for this analysis is arbitrary.

Figure 20 presents a part of the g-f-V diagram for case 45, from Fig. 16b, but for low frequency, f and negative damping factor, g.

Mode 8 (frequency 2.15 Hz) is very damped and does not contain any sticks movement. The mode 7 (frequency 1.41 Hz, Fig. 20c) is damped, but contains lateral stick movement with phase shift, so it does exist the possibility to induce it by active pilot's reaction.

7 Conclusions

The wing torsion-bending flutter behavior is typical for swept wing aircraft. The wing torsional stiffness of the EM-12 appears as sufficient. Even though the structural damping was not included, the safety margin between calculated critical flutter speed and V_D is more than 30%. The safety margin should be greater due to atypical scheme of the EM-12 aircraft and uncertainty of computational model. The flutter computation results can be sensitive to data changes - only a couple of these parameters were examined.

No instability modes with dominant participation of canard forward surface deflection were detected, but the used computational method does not take nonlinearities into account.

The forward surface of EM-12 aircraft is controlled by tabs located behind elastic axis. According to computational results, the addition of tabs mass balance and/or the increase of the tabs mass is reducing the critical speed of anti-symmetric torsional flutter of forward surfaces. In these cases the maximal speed of aircraft should be limited to 210 km/h (tab solution on Fig. 11b) or 240 km/h (tab solution on Fig. 11c) - at maximum. The speed limits are formulated based on results presented on Figures 12 and 16 (where the structural damping is not taken into account) and speed safety margin more than 20%. Generally, the heavy canard tabs are unfavourable for aeroelastic properties of the aeroplane.

In the special aircraft category the analysis of flutter properties after failure is not required, so this analysis is not provided. Each failure, especially canard or tab support failure, can be dangerous.

References

[1] R. Rosenbaum. Simplified Flutter Prevention Criteria for Personal Type Aircraft. *Airframe and Equipment Engineering Report No. 45.*

[2] W. Stender and F. Kiessling. Aeroelastic Flutter Prevention in Gliders and Small Aircraft. *DLR-Mitteilung 91-03*, 1991.

[3] W. Chajec. Critical Flutter Speed of Sailplanes Calculated for High Altitude. *Examples of Computation, Technical Soaring, Vol XVIII, No. 3, 69-72,*, 1993.

[4] W. Chajec. Aeroelastic Analyses in PZL-Mielec Using MSC/NASTRAN. *MSC Worldwide Aerospace Conference, Long Beach, CA*, 1999.

[5] Various Authors. Final Report on Optimized Analytical and Experimental Approaches and Improved Methods for Reliable and Fast Prediction of Aeroelastic Stability, Deliverable D 2.5.1/2-3. *CESAR-Cost-Effective Small AiRcraft*, 2010.

[6] Z. Goraj and W. Chajec. Aeroelastic Analysis of Remotely Controlled Research Vehicles with numerous control surfaces. *International Journal of Structural Integrity, Vol. 2. No. 2, 158-184*, 2011.

[7] W. Chajec and T. Seibert. Flutter Calculation Based on GVT-results and Theoretical Mass Model. *IFASD-2011-186, Paris*, 2011.